Discover Nano

Research

Interference between multipolar two-photon transitions in quantum emitters near plasmonic nanostructures

S. Smeets[1] · **B. Maes**[1] · **G. Rosolen**[1]

Received: 16 May 2024 / Accepted: 11 September 2024
Published online: 27 September 2024

Abstract
In the vicinity of plasmonic nanostructures that support highly confined light fields, spontaneous emission processes, such as two-photon spontaneous emission (TPSE), exhibit higher-order multipolar emission pathways beyond the dipolar one. These multipolar emission channels occur simultaneously and can interfere with each other. We develop a novel framework that computes these interference effects for TPSE of a quantum emitter close to an arbitrary nanostructure. The model is based on the computation of Purcell factors that can be calculated with conventional electromagnetic simulations, which avoids complex analytic calculations for the environment. For a transition of a hydrogen-like emitter close to a graphene nanotriangle, we demonstrate a breakdown of the dipolar selection rule in the TPSE process. This breakdown is due to a huge enhancement of the two-electric dipole (2ED) and of the two-electric quadrupole (2EQ) transitions. We observe an important interference between these multipolar transitions, as it increases the total rate by 67 %. In the end, our framework is a complete tool to design emitters and nanostructures for TPSE, where the exploitation of previously ignored interference effects provides an additional degree of freedom, for example to boost desired transitions and to supress undesirable ones.

Keywords Two-photon spontaneous emission · Interference · Dipole approximation breakdown · Plasmonic nanostructure · Framework · Purcell factor

1 Introduction

Two-photon spontaneous emission (TPSE) is a broadband second-order process in the field of light-matter interaction that involves the simultaneous emission of two photons from a quantum emitter. Enhancing and tailoring this process is of great interest, as it promises several applications [1, 2], for example as an alternative to conventional entangled photon pair sources using the parametric down-conversion process in nonlinear crystals [3] for quantum applications [4–7]. Since its prediction in 1931 [8], this second-order process has been investigated in many systems, such as in atoms [9–11], molecules [12], quantum dots [13–15], semiconductors [4, 16–18], epsilon-near-zero-materials [19], plasmonic nanostructures [2, 20, 21], and cosmic strings [22].

Despite the interest in controlling the TPSE process [23], it typically occurs 8 to 10 orders of magnitude slower than the competing spontaneous emission of a single photon [24]. However, electromagnetic interactions with the surrounding environment are known to modify spontaneous emission rates of quantum emitters: the Purcell effect [25,

✉ S. Smeets, Steve.Smeets@umons.ac.be; B. Maes, Bjorn.Maes@umons.ac.be; G. Rosolen, Gilles.Rosolen@umons.ac.be | [1]Micro- and Nanophotonic Materials Group, Research Institute for Materials Science and Engineering, University of Mons, 20 Place du Parc, 7000 Mons, Belgium.

26]. Specifically, when the electromagnetic field is confined at the nanometer scale, such as in plasmonic nanostructures [27–36], there is a light emission enhancement by several orders of magnitude [24, 37]. Moreover, higher-order transitions can be enhanced and even outperform the electric dipole single-photon transition, leading to multiquanta and multipolar transitions [24, 27, 36]. For example, a local breakdown of the dipole selection rule was calculated for a hydrogen-like emitter near graphene nanoislands, where the one-photon quadrupolar transition rate becomes 100 times larger than the dipolar one [36].

Allowed transitions between two given states of a quantum emitter are dictated by selection rules [38]. Between two states of an atom, there is only one possible decay channel for the emission of a single photon (e.g., electric dipole, magnetic dipole, electric quadrupole, etc.) [38], and therefore no interference. However in the TPSE process, the second-order transition is mediated by virtual intermediate states, allowing multiple multipolar emission channels to exist simultaneously [39]. For example, in vacuum and for a $2s \rightarrow 1s$ transition in hydrogen, the two-electric dipole (2ED), two-magnetic dipole (2MD), and two-electric quadrupole (2EQ) multipolar emission channels occur simultaneously, however, with the 2MD and 2EQ transition being twelve and thirteen orders of magnitude slower than the 2ED one, respectively [39]. Unlike in vacuum, inside a photonic environment the multipolar field distributions are modified and interference between multipolar emission channels can occur, leading to an increase or decrease of the total transition rate [40]. Thereby, if in a system (atom plus environment) several multipolar two-photon emission channels are of the same order magnitude and are responsible for the emitter transition rate, it is necessary to take into account the interference effects among the dominant channels [40]. Note that in the case of molecules and asymmetric quantum dots, multiple multipolar single-photon emission channels can occur simultaneously, and therefore can interfere. For example, interference effects were studied between the one-photon magnetic dipole and electric quadrupole transitions in molecules [37] and between one-photon electric dipole, magnetic dipole and electric quadrupole transitions in quantum dots [41], but never between two-photon multipolar transitions to our knowledge.

In this paper we study the interference effects between the two-photon multipolar emission channels of an atom near a plasmonic nanostructure. For this purpose we add the interference terms to our framework [42] that computes the TPSE rate of a quantum emitter at any position, close to an arbitrary structure, and beyond the dipolar approximation by considering interactions up to the electric quadrupolar order. The framework relies on the analytical calculation of the emitter contribution and on the classical computation of one-photon Purcell factors by modeling classical point emitters in electromagnetic simulations for the environment contribution, which allows the consideration of complex geometries without available analytical models. In comparison with the formula derived by Muniz et al. [43] to calculate the 2ED transition rate, for example near plasmonic nanostructures [20] and in cosmic strings [22], the formula we derive contains additional terms that are linked to the off-diagonal components of the Green's function, and it is therefore more general [42]. Note that our framework is based on Fermi's golden rule and is therefore limited to the weak-coupling regime [42]. Furthermore, for the extreme case of large emitters (larger than 1 nm) placed very close to a nanostructure ($\approx$ 1 nm distance), their reduction to a point may require even higher orders than the quadrupolar order [44]. Then, we calculate the interference effects between the 2ED and 2EQ emission channels for a $5s \rightarrow 3s$ transition in a hydrogen-like emitter near a graphene nanotriangle, where the results show a breakdown of the dipole approximation in the TPSE process and an important increase of the total two-photon transition rate due to the interference between the two decay channels. In order to carry out this study we needed to calculate the 2ED and 2EQ transition rates in vacuum, which were not reported before (see Section III of the Supporting Information).

First, in the method section, we derive the interference term that we write as a function of the one-photon Purcell factors. Then we develop the methods used to calculate the emitter contribution as well as the Purcell factors, and the method section ends with a concluding discussion. Next in the results and discussion section, our extended framework is used to study the interference effects between the 2ED and 2EQ emission channels of a hydrogen-like emitter near a graphene nanotriangle.

2 Method

Previously we established a link between the TPSE rate of an emitter and the Purcell factors of the one-photon spontaneous emission process [42]. This connection was derived for the 2ED, 2MD and 2EQ transitions and holds true regardless of the emitter and its environment. Here, we extend this connection with additional terms that account for interference

effects between the two-photon multipolar emission channels. In particular, as the 2MD transition is negligible near a graphene nanotriangle, we focus on the interaction between the 2ED and 2EQ transitions.

We start with the Hamiltonian that characterizes the interactions between the emitter and the electromagnetic field, followed by an examination of the multipolar contributions, including interferences, to the overall TPSE process. Next, we provide the expression for the total TPSE rate that is derived using the second-order Fermi's golden rule, and we introduce the term describing interference between the 2ED and 2EQ emission channels. Subsequently, we express the interference term as a function of the dyadic Green's function, we establish the link with the one-photon Purcell factors, and we discuss the derived formulas. Note that Section I of the Supporting Information (SI) contains the full developments leading to the presented equations. Finally, our methods to calculate the emitter contribution and the Purcell factors are explained and we end with a conclusion on the method.

2.1 Interaction Hamiltonian

We consider the interaction Hamiltonian up to the electric quadrupolar order [26, 45]:

$$H_{\text{int}}(\mathbf{R},t) = \underbrace{-\mathbf{d}\cdot\mathbf{E}(\mathbf{R},t)}_{H_{\text{ED}}}\underbrace{-\mathbf{Q}:[\nabla\mathbf{E}(\mathbf{R},t)]}_{H_{\text{EQ}}}, \tag{1}$$

where the emitter position $\mathbf{R}$ is taken at the center of its charge distribution, and where the magnetic dipolar interaction is discarded since the structure considered later is not relevant to enhance this interaction [33, 46]. $\nabla = (\frac{\partial}{\partial x}, \frac{\partial}{\partial y}, \frac{\partial}{\partial z})^T$ represents a column vector with T indicating the transpose operation, the dot product denotes the scalar product of vectors, while the product $\nabla\mathbf{E}$ is an outer product. Additionally, the double dot product is defined as $\mathbf{T}:\mathbf{U} := \sum_{i,j} T_{\ldots ij} U_{ji\ldots}$ with $\mathbf{T}$ and $\mathbf{U}$ two tensors of rank greater than or equal to two. Moreover, $\mathbf{d}$ and $\mathbf{Q}$ are, respectively, the electric dipole (ED) and the electric quadrupole (EQ) moment operators, while $\mathbf{E}$ is the electric field operator that can be written as a function of the normal modes $\mathbf{A}_\alpha(\mathbf{r})$ [42, 47, 48].

In the second-order TPSE process the total transition rate $\Gamma^{(2)}_{\text{tot}}$ results from three multipolar contributions:

$$\Gamma^{(2)}_{\text{tot}} \approx \Gamma^{(2)}_{\text{2ED+2EQ}} = \Gamma^{(2)}_{\text{2ED}} + \Gamma^{(2)}_{\text{2EQ}} + \Gamma^{(2)}_{\text{2ED}\cap\text{2EQ}}, \tag{2}$$

where the superscript (2) indicates second-order transitions, where the spatial dependency has been omitted, and with $\Gamma^{(2)}_{\text{2ED+2EQ}}$ being the total transition rate due to the 2ED and 2EQ transitions. On the one hand, there are the 2ED and 2EQ transitions, under which both photons are emitted via the same multipolar first-order transition. Note that there are also the mixed transitions ED–EQ and EQ–ED in which the photons originate from different multipolar first-order transitions. However, these are not considered here as they are not allowed between two states of an hydrogen atom that have the same azimuthal quantum number [38, 39]. On the other hand, there is the interference term $\Gamma^{(2)}_{\text{2ED}\cap\text{2EQ}}$ describing the interference among the 2ED and 2EQ emission channels [40]. Note that the interference term can be either positive or negative, potentially resulting in an increase or decrease of the overall TPSE rate.

2.2 Total two-photon spontaneous emission rate

Using the interaction Hamiltonian [Eq. (1)] in the second-order Fermi's golden rule [40], the total TPSE rate can be expressed as follows (see the SI and Fig. 1):

$$\Gamma^{(2)}_{\text{2ED+2EQ}}(\mathbf{R}) = \frac{\pi}{4\epsilon_0^2\hbar^2}\sum_{\alpha,\alpha'}\omega_\alpha\omega_{\alpha'}\left|\mathbf{A}_\alpha\cdot\boldsymbol{\mathcal{D}}^{eg}\cdot\mathbf{A}_{\alpha'} + \nabla\mathbf{A}_\alpha : \boldsymbol{\mathcal{Q}}^{eg} : \nabla\mathbf{A}_{\alpha'}\right|^2\delta(\omega_{eg}-\omega_\alpha-\omega_{\alpha'}), \tag{3}$$

where the summations run over the modes α and α' of the two emitted quanta during this process. ϵ_0 is the vacuum electric permittivity, ω_α denotes the angular frequency of the photon in the mode α, δ represents the Dirac delta distribution, and $\hbar\,\omega_{eg}$ corresponds to the transition energy between the excited and the ground state of the emitter, with $\hbar$ the reduced Planck constant. We have omitted the spatial dependency of the field modes $\mathbf{A}_\alpha(\mathbf{R})$, as well as the frequency dependency of the second-order transition electric dipole and quadrupole moments, defined as [40, 42]:

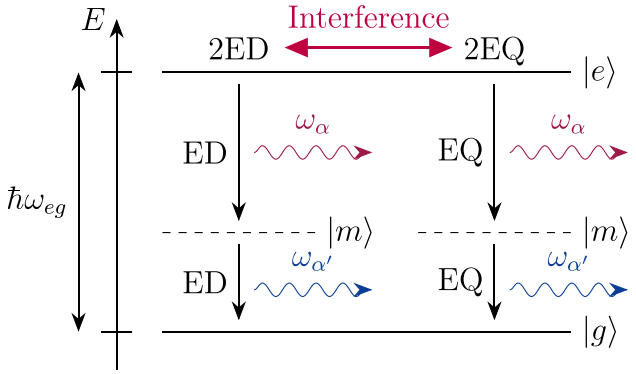

Fig. 1 Energy representation of a second-order transition. The emitter carries out a first transition from its excited state $|e\rangle$ to a virtual intermediate state $|m\rangle$ by emitting a photon in the mode α. Then, a second transition is carried out to the ground state $|g\rangle$ of lower energy by emitting a photon in the mode α'. The emitter performs either a 2ED or a 2EQ transition that interfere, leading to three contributions to the total transition rate [Eq. (2)]. The 2ED and 2EQ transitions are mediated by different intermediate states. In the case of a transition between two *s* states (characterized by an azimuthal quantum number *l*=0), the 2ED transition is mediated by *p* states ($l = 1$), while the 2EQ transition is mediated by *d* states ($l = 2$) [39]. The law of conservation of energy implies that the energy of the two photons is equal to the transition energy: $\hbar\omega_\alpha + \hbar\omega_{\alpha'} = \hbar\omega_{eg}$. A similar representation can be sketched by inverting the role of the two emitted quanta

$$\mathcal{D}^{eg}(\omega_\alpha,\omega_{\alpha'}) := \sum_{|m\rangle}\left(\frac{\mathbf{d}^{em}\mathbf{d}^{mg}}{\omega_{em}-\omega_\alpha}+\frac{\mathbf{d}^{mg}\mathbf{d}^{em}}{\omega_{em}-\omega_{\alpha'}}\right), \tag{4a}$$

$$\mathcal{Q}^{eg}(\omega_\alpha,\omega_{\alpha'}) := \sum_{|m\rangle}\left(\frac{\mathbf{Q}^{em}\mathbf{Q}^{mg}}{\omega_{em}-\omega_\alpha}+\frac{\mathbf{Q}^{mg}\mathbf{Q}^{em}}{\omega_{em}-\omega_{\alpha'}}\right), \tag{4b}$$

where the outer product is implied. These tensors represent the emitter contribution and their definitions involve a summation over the virtual intermediate states $|m\rangle$ of the emitter that connect, via the selection rules, the initial state to the final one. $\hbar\omega_{em}$ is the energy difference between the excited and intermediate states of the emitter. These second and fourth rank tensors describe the two successive electric dipole and electric quadrupole transitions, respectively, between the excited $|e\rangle$ state and the ground state $|g\rangle$ of the emitter. These consecutive transitions, assisted by a virtual intermediate state and each emitting a quantum, are described by the first-order electric dipole and quadrupole moments, denoted as $\mathbf{d}^{ab}$ and $\mathbf{Q}^{ab}$. Note that in the case of an $s \to s$ two-photon transition, the summation over $|m\rangle$ denotes a summation over the principal and the magnetic quantum numbers of the intermediate states (see Sec. III of the SI), the azimuthal quantum number being fixed (see caption of Fig. 1).

From equation (3), the interference term of equation (2) can be written as (see the SI):

$$\Gamma^{(2)}_{\mathrm{2ED}\cap\mathrm{2EQ}}(\mathbf{R}) = 2\,\mathrm{Re}\left(\frac{\pi}{4\epsilon_0^2\hbar^2}\sum_{\alpha,\alpha'}\omega_\alpha\omega_{\alpha'}\left(\mathbf{A}_\alpha\cdot\mathcal{D}^{eg}\cdot\mathbf{A}_{\alpha'}\right)\left(\nabla\mathbf{A}_\alpha\,:\,\mathcal{Q}^{eg}\,:\,\nabla\mathbf{A}_{\alpha'}\right)^*\delta(\omega_{eg}-\omega_\alpha-\omega_{\alpha'})\right), \tag{5}$$

where Re stands for the real part, which will be omitted hereafter for clarity. In vacuum the interference term vanishes [40]. The 2ED and 2EQ terms in equation (2) are given in Ref. [42] and in the SI.

2.3 Interference term via the Green's function

To derive an expression for the interference term that relies on one-photon Purcell factors, we first normalize it with the 2ED and 2EQ transition rates in vacuum, and then we rewrite it as a function of the dyadic Green's function [26, 42]. We obtain (see the SI):

$$\Gamma^{(2)}_{\text{2ED}\cap\text{2EQ}}(\mathbf{R}) = \int_0^{\omega_{eg}} \gamma^{(2)}_{\text{2ED}\cap\text{2EQ}}(\omega;\mathbf{R})\,\mathrm{d}\omega, \tag{6}$$

with the spectral distribution rate of the emitted quanta

$$\frac{\gamma^{(2)}_{\text{2ED}\cap\text{2EQ}}(\omega;\mathbf{R})}{\sqrt{\gamma^{(2)}_{\text{2ED},0}(\omega)\,\gamma^{(2)}_{\text{2EQ},0}(\omega)}} = 2\,\hat{\mathcal{D}}^{eg}_{ia}(\omega,\omega_{eg}-\omega)\left[\hat{\mathcal{Q}}^{eg}_{jkbc}(\omega,\omega_{eg}-\omega)\right]^{*} T_{ijk}(\omega;\mathbf{R})\,T_{abc}(\omega_{eg}-\omega;\mathbf{R}). \tag{7}$$

The Einstein summation convention is used, the caret indicates normalized tensors (i.e., for an n^{th} rank tensor $\mathbf{U}$ with $n \in \mathbb{N}_0$, $\hat{\mathbf{U}} := \mathbf{U}/\|\mathbf{U}\|$ with $\|\mathbf{U}\|^2 := \sum_{i_1,i_2,\ldots,i_n} \left|U_{i_1,i_2,\ldots,i_n}\right|^2$.). $\gamma^{(2)}_{\text{2ED},0}$ and $\gamma^{(2)}_{\text{2EQ},0}$ are respectively the 2ED and 2EQ vacuum transition rates, whose expressions are given in Ref. [42] and calculated in the SI for $s \to s$ transitions. Furthermore, the third rank tensor $\mathbf{T}$ is defined as a function of the imaginary part of the Green's function:

$$T_{ijk}(\omega;\mathbf{R}) := \frac{2\sqrt{30}\pi c^2}{\omega^2}\left\{\partial_{k'}\,\mathrm{Im}\,G_{ij}(\omega;\mathbf{r},\mathbf{r}')\right\}_{\mathbf{r}=\mathbf{r}'=\mathbf{R}'} \tag{8}$$

where $\partial_{k'}$ means derivative with respect to the coordinates of $\mathbf{r}'$. Hence, the interference term involves the first derivatives of the imaginary part of the Green's function [41], and is related to the power emitted by an electric point dipole and an electric point quadrupole at the same position (See Section II of the SI). Similarly, the 2ED transition is related to Im $\mathbf{G}$ or the power emitted by dipolar point sources [26], while the 2EQ transition is related to the double derivative of Im $\mathbf{G}$ or the power emitted by quadrupolar point sources [23, 41, 42]. Note that the first tensor $\mathbf{T}$ in equation (7) is related to the quanta emitted at the frequency ω, while the second one concerns the complementary frequency $\omega_{eg} - \omega$.

The derived equation (7) contains 3^6 terms, but fortunately we can leverage the properties of the tensor $\mathcal{Q}^{eg}$ derived from the symmetric and traceless properties of electric quadrupole moments to eliminate redundant terms. This reduction results in a formula involving $3^2 \times 5^2$ terms (see the SI):

$$\frac{\gamma^{(2)}_{\text{2ED}\cap\text{2EQ}}(\omega;\mathbf{R})}{\sqrt{\gamma^{(2)}_{\text{2ED},0}(\omega)\,\gamma^{(2)}_{\text{2EQ},0}(\omega)}} = 2\sum_{i,j=1}^{3}\sum_{\mu,\nu=1}^{5} \hat{\mathcal{D}}^{eg}_{ij}(\omega,\omega_{eg}-\omega)\left[\hat{\mathcal{Q}}^{eg}_{\mu\nu}(\omega,\omega_{eg}-\omega)\right]^{*} F_{i\mu}(\omega;\mathbf{R})\,F_{j\nu}(\omega_{eg}-\omega;\mathbf{R}), \tag{9}$$

where the superscript of the second rank tensor $\mathbf{F}^{\text{ED}\cap\text{EQ}}$, which is expressed as a function of the tensor $\mathbf{T}$, has been omitted. The first index in Latin letter and the second one in Greek letter of this Tensor are related, respectively, to the second-order electric dipole and electric quadrupole transition moments. This formula was obtained by employing a modified Voigt notation that allows to rewrite the tensor $\mathcal{Q}^{eg}$ as a second-rank tensor in five dimensions after removing redundant components arising from the symmetry and traceless properties [42].

2.4 Interference term as a function of Purcell factors

In the weak-coupling regime, the Purcell factor is defined as the ratio between the one-photon transition rate of a quantum emitter in a given photonic environment and in vacuum, $P := \Gamma^{(1)}/\Gamma^{(1)}_0$, which can be calculated by considering classical radiating point sources [26]. In the case where multiple multipolar emission channels contribute to the transition rate, the classical source is described by the superposition of multipolar point sources, with multipolar moments identical to the multipolar transition moments of the emitter. In the TPSE process, the two-photon Purcell effect can be written as a weighted summation of the product between the one-photon Purcell factors of the two emitted quanta, where the summation runs over different source orientations (see the SI).

The total spectral TPSE rate is split into three contributions [Eq. (2)]:

$$\gamma^{(2)}_{\text{2ED+2EQ}}(\omega;\mathbf{R}) = \gamma^{(2)}_{\text{2ED}} + \gamma^{(2)}_{\text{2EQ}} + \gamma^{(2)}_{\text{2ED}\cap\text{2EQ}}, \tag{10}$$

where the 2ED and 2EQ contributions have been written as function of one-photon Purcell factors in Ref. [42], and where the interference term (which we want to express as a function of the Purcell factors) is given in equation (9).

To link with the Purcell factors, the idea is to assume specific directions for the first-order multipolar transition moments involved in the definition of the second-order multipolar transitions moments [Eq. (4)]. Since general electric dipole and

quadrupole moments involve, respectively, up to three and five independent components, they can be expanded with an orthonormal basis of 3 dipoles and 5 quadrupoles. For the dipolar moments, these are the three basis vectors, while for the quadrupolar ones, the basis is built from two different types of planar quadrupoles [42]. Type I ($\hat{\mathbf{Q}}_{yz}$, $\hat{\mathbf{Q}}_{xz}$, and $\hat{\mathbf{Q}}_{xy}$) involve solely off-diagonal components, while Type II ($\hat{\mathbf{Q}}_{xx}$ and $\hat{\mathbf{Q}}_{yy}$) involves only diagonal components and differs from type I by an in-plane rotation of 45° [42]. In our adapted Voigt notation, these quadrupoles are represented by a five dimensional vector in which only the μ-th component is non-zero and equals to $1/\sqrt{2}$.[1]

Let us take the two first-order electric dipole transition moments aligned along one basis vector, i.e., $\hat{\boldsymbol{d}}^{em} = \hat{\boldsymbol{d}}^{mg} = \hat{\mathbf{e}}_i$ with $i = 1, 2, 3$, and the two first-order electric quadrupole transition moments aligned along one basis vector, i.e., $\hat{\boldsymbol{Q}}^{em} = \hat{\boldsymbol{Q}}^{mg} = \hat{\mathbf{e}}_\mu/\sqrt{2}$ with $\mu = 1, \ldots, 5$. In this case, using equations (4), the normalized second-order multipolar transition moments are given by

$$\hat{\mathcal{D}}^{eg} = \hat{\mathbf{e}}_i \hat{\mathbf{e}}_i, \tag{11a}$$

$$\hat{\mathcal{Q}}^{eg} = \frac{1}{2}\,\hat{\mathbf{e}}_\mu \hat{\mathbf{e}}_\mu. \tag{11b}$$

Therefore, using the equations in Ref. [42] for the 2ED and 2EQ terms, equation (9) for the interference term, and equations (11) for the multipolar moments, the total transition rate given by equation (10) is rewritten as

$$\gamma^{(2)}_{\mathrm{2ED+2EQ}} = \gamma^{(2)}_{\mathrm{2ED},0}\, P_i^{\mathrm{ED}} P_i'^{\mathrm{ED}} + \gamma^{(2)}_{\mathrm{2EQ},0}\, P_\mu^{\mathrm{EQ}} P_\mu'^{\mathrm{EQ}} + 2\sqrt{\gamma^{(2)}_{\mathrm{2ED},0}\,\gamma^{(2)}_{\mathrm{2EQ},0}}\,\frac{1}{2}\,F_{i\mu}^{\mathrm{ED}\cap\mathrm{EQ}} F_{i\mu}'^{\mathrm{ED}\cap\mathrm{EQ}}, \tag{12}$$

where the dependencies have been omitted. P_i^{ED} and P_μ^{EQ} correspond to the Purcell factors related to an electric dipole aligned along $\hat{\mathbf{e}}_i$ and to an electric quadrupole aligned along $\hat{\mathbf{e}}_\mu$ [42], respectively. For clarity we adopt the following notation: without prime denotes an evaluation at ω, with prime means the complementary frequency $\omega_{eg} - \omega$.

The left-hand side of the last equation $\gamma^{(2)}_{\mathrm{2ED+2EQ}}$ can also be written as a function of the product between two Purcell factors: $P_{i\mu}^{\mathrm{ED+EQ}} P_{i\mu}'^{\mathrm{ED+EQ}}$, with $P_{i\mu}^{\mathrm{ED+EQ}}$ being the Purcell factor related to an electric dipole aligned along $\hat{\mathbf{e}}_i$ plus an electric quadrupole aligned along $\hat{\mathbf{e}}_\mu$ (see the SI). However, this left-hand side also contains the mixed transitions ED–EQ and EQ–ED, which have been discarded in the right-hand side in our developments based on Fermi's golden rule. Therefore, by removing the mixed transition contributions in the left-hand side and by noticing that the interference terms describing the interaction between the 2ED and 2EQ transitions and between the mixed transitions ED–EQ and EQ–ED are identical,[2] we obtain an expression for the tensor $\mathbf{F}^{\mathrm{ED}\cap\mathrm{EQ}}$ as a function of the one-photon Purcell factors (see the SI):

$$\left(\gamma^{(2)}_{\mathrm{2ED},0}\,\gamma^{(2)}_{\mathrm{2EQ},0}\right)^{1/4} F_{i\mu}^{\mathrm{ED}\cap\mathrm{EQ}} = \frac{1}{\sqrt{2}}\left[\left(\sqrt{\gamma^{(2)}_{\mathrm{2ED},0}} + \sqrt{\gamma^{(2)}_{\mathrm{2EQ},0}}\right) P_{i\mu}^{\mathrm{ED+EQ}} - \sqrt{\gamma^{(2)}_{\mathrm{2ED},0}}\, P_i^{\mathrm{ED}} - \sqrt{\gamma^{(2)}_{\mathrm{2EQ},0}}\, P_\mu^{\mathrm{EQ}}\right], \tag{13}$$

where the dependencies have been omitted. Note that in vacuum, all Purcell factors tend towards one and the tensor $\mathbf{F}^{\mathrm{ED}\cap\mathrm{EQ}}$ tends, as expected, towards zero, leading to an interference term [Eq. (9)] equal to zero.

The Purcell factors involved in the last equation can be calculated via the power emitted by classical point sources [26]:

$$P_i^{\mathrm{ED}} = \frac{W_i^{\mathrm{ED}}}{W_0^{\mathrm{ED}}}, \qquad P_\mu^{\mathrm{EQ}} = \frac{W_\mu^{\mathrm{EQ}}}{W_0^{\mathrm{EQ}}}, \tag{14a}$$

$$P_{i\mu}^{\mathrm{ED+EQ}} = \frac{W_{i\mu}^{\mathrm{ED+EQ}}}{W_0^{\mathrm{ED}} + W_0^{\mathrm{EQ}}}, \tag{14b}$$

[1] The factor $1/\sqrt{2}$ for the quadrupoles is the normalization factor for quadrupoles that are described by two equal components in absolute value.

[2] Indeed, both situations are identical from an interference point of view, since it is always an interaction between an ED and EQ emission channel, leading to the same tensor $\mathbf{F}^{\mathrm{ED}\cap\mathrm{EQ}}$ and to the same interference term.

where the subscript 0 indicates quantities that refer to vacuum. W_i^{ED}, W_μ^{EQ}, and $W_{i\mu}^{\mathrm{ED+EQ}}$ denote the power emitted by a classical dipole aligned along $\hat{\mathbf{e}}_i$, by a classical quadrupole aligned along $\hat{\mathbf{e}}_\mu$, and by the superposition of both sources, respectively. Note that $W_{i\mu}^{\mathrm{ED+EQ}}$ contains the interference term between the ED and EQ point sources and that there is no interference in vacuum. In addition, to calculate $W_{i\mu}^{\mathrm{ED+EQ}}$, the power emitted by the classical multipolar sources representing the multipolar transition moments of the emitter need to be set according to the two-photon multipolar transition rates in vacuum:

$$\frac{W_0^{\mathrm{EQ}}}{W_0^{\mathrm{ED}}} = \sqrt{\frac{\gamma_{2\mathrm{EQ},0}^{(2)}}{\gamma_{2\mathrm{ED},0}^{(2)}}}. \tag{15}$$

In the most general case, 3 Purcell factors P_i^{ED}, 3 Purcell factors P_μ^{EQ}, and 15 Purcell factors $P_{i\mu}^{\mathrm{ED+EQ}}$ are necessary to calculate the 15 components of the tensor $F^{\mathrm{ED}\cap\mathrm{EQ}}$ involved in the interference term of the equation (9). Note that the Purcell factors P_i^{ED} and P_μ^{EQ} are already calculated when calculating the 2ED and 2EQ transition rates [42]. Depending on the symmetry of the studied photonic environment, the coordinate basis can be chosen so that some Purcell factors are equal, thus reducing the number of Purcell factors to calculate. For example, in the case of an azimuthal symmetry around the z axis: $P_x^{\mathrm{ED}} = P_y^{\mathrm{ED}}$.

2.5 Calculation of the emitter contribution

To calculate the interference term given by equation (9), one first needs to calculate the emitter contribution: the second-order transitions moments and the rates in vacuum. This is done analytically for the $5s \rightarrow 3s$ transition in hydrogen via the wave functions of the emitter. The related transition energy is $\hbar\omega_{eg} = 0.967$ eV, which corresponds to a wavelength of 1.28 µm. The normalized second-order transition moments have been calculated analytically for $s \rightarrow s$ transitions in Refs. [42, 43] and are independent of the frequencies of the emitted quanta:

$$\hat{\mathcal{D}}^{eg} = \frac{\mathbb{1}_3}{\sqrt{3}}, \tag{16a}$$

$$\hat{\mathcal{Q}}^{eg} = \frac{1}{\sqrt{20}} \begin{pmatrix} 4/3 & -2/3 & 0 & 0 & 0 \\ -2/3 & 4/3 & 0 & 0 & 0 \\ 0 & 0 & 1 & 0 & 0 \\ 0 & 0 & 0 & 1 & 0 \\ 0 & 0 & 0 & 0 & 1 \end{pmatrix} \tag{16b}$$

where $\mathbb{1}_3$ is the identity matrix in three dimensions.

To calculate the vacuum 2ED and 2EQ transition rates, we employ the method by Chluba and Sunyaev [49, 50] in their calculation of 2ED transition spectra for the $ns \rightarrow 1s$ and $nd \rightarrow 1s$ transitions in hydrogen. Moreover, we used the analytical expression derived by Matsumoto [51] for the multipole matrix elements to extend the method to the 2EQ transition. The detailed calculation is presented in Section III of the SI. Thus, the vacuum TPSE rate related to the multipolar operator $\mathrm{MO} \in \{\mathrm{ED}, \mathrm{EQ}\}$ can be written as follows:

$$\Gamma_{2\mathrm{MO},0}^{(2)} = \int_0^{\omega_{eg}} \gamma_{2\mathrm{MO},0}^{(2)}(\omega)\,\mathrm{d}\omega = \int_0^{1/2} \phi_{2\mathrm{MO},0}^{(2)}(y)\,\mathrm{d}y \tag{17}$$

where $\phi_{2\mathrm{MO},0}^{(2)}(y) = 2\,\omega_{eg}\,\gamma_{2\mathrm{MO},0}^{(2)}(\omega)$ and where $\phi_{2\mathrm{MO},0}^{(2)}(y)\,\mathrm{d}y$ denotes the number of photons emitted per second in the frequency interval between y and $y + \mathrm{d}y$, with $y := \omega/\omega_{eg}$ the dimensionless frequency comprised between 0 and 1 [49]. The latter emission profile encompasses the photons emitted simultaneously during this second-order process at complementary frequencies, necessitating integration over only half of the spectrum.[3] Furthermore, the probability of

[3] The definition of $\gamma_{2\mathrm{MO},0}^{(2)}(\omega)$ does not count the quanta emitted simultaneously at complementary frequencies, which explains the factor 2 difference with the definition of the emission profile $\phi_{2\mathrm{MO},0}^{(2)}(y)$.

emitting a photon at one frequency is equal to the probability of emitting a photon at the complementary frequency, leading to symmetric spectra with respect to $\omega = \omega_{eg}/2$ [49]. For the $5\,s \rightarrow 3\,s$ transition, we obtained the following values: $\Gamma^{(2)}_{\mathrm{2ED},0} = 1.18 \times 10^{-2}\,\mathrm{s}^{-1}$, $\phi^{(2)}_{\mathrm{2ED},0}(1/2) = 3.24 \times 10^{-2}\,\mathrm{s}^{-1}$, $\Gamma^{(2)}_{\mathrm{2EQ},0} = 1.43 \times 10^{-15}\,\mathrm{s}^{-1}$, $\phi^{(2)}_{\mathrm{2EQ},0}(1/2) = 5.96 \times 10^{-15}\,\mathrm{s}^{-1}$. These values are in agreement with the ones available in the literature (see the SI) [39, 49].

2.6 Computation of Purcell factors

To calculate the three contributions to the total two-photon transition rate [Eq.(10)], one then needs to compute Purcell factors of multipolar point sources at different frequencies. Specifically, we use COMSOL Multiphysics®, which is based on the finite element method, but any other electromagnetic tool can be employed. In total, there are 6 Purcell factors to calculate the 2ED transition rate by modeling electric point dipoles [42], 15 to calculate the 2EQ transition rate by modeling electric point quadrupoles [42], and 15 to calculate the interference by modeling the superposition of the two electric multipole point sources [Eqs. (9) and (13)]. They correspond to different source orientations and their computation is carried out over a range of frequencies. All these source orientations are required because the emitter is spherically symmetric (see the calculated transition moments in Eqs. (16)). Furthermore, when simulating superposition of multipolar sources at the same position, the power emitted by the classical sources is chosen in such a way that equation (15) is verified, which allows to account for the branching fraction of the multipolar emission channels. In addition, due to the expression of the electric dipole and quadrupole moment operators [45], the electric dipole moments are in phase with the electric quadrupole ones. The expression of the free-space emitted power for point sources can be found in Ref. [52].

Inside a photonic environment, a quantum emitter can decay either radiatively in the case of emission of photons (energy radiated in the far-field) or non-radiatively in the case of energy dissipation in the environment, for example in the form of plasmons or phonons [26]. Near plasmonic nanostructures, the non-radiative channel is dominated by the excitation of plasmons. This decomposition into three pathways is valid for the 2ED and 2EQ transitions. As a result, the two-quanta spontaneous emission process is given by three distinct emission pathways: the photon-photon (ph-ph), photon-plasmon (ph-pl), and plasmon-plasmon (pl-pl) emission channels, which can be calculated through the decomposition of the Purcell factors into radiative and non-radiative parts.

The parameters of our COMSOL models to compute in the frequency domain the Purcell factors for the hydrogen-like emitter under the graphene nanotriangle [Fig. 2a, b] are as follows. First, the simulation domain is a sphere with a radius equal to half the studied wavelength λ, and perfectly matched layers (PMLs) are defined as an outer layer with a thickness of $\lambda/8$. Second, the graphene nanotriangle is modeled using a transition boundary condition [53] applied to a two-dimensional equilateral triangle with rounded corners of 2 nm, an effective thickness of $t = 0.335$ nm [54], and a side length C ranging from 10 to 80 nm. Its optical response is characterized by a 2D surface conductivity [55, 56] that is given in Section IV of the SI. Thus, the graphene optical response can be tuned via its Fermi energy E_F, i.e., the doping level. Third, the classical emitter is positioned 2 nm under the nanotriangle and is modelled by a radiating electric point dipole, quadrupole, or the superposition of both. We implemented the weak formulation of the electric point quadrupole: $-j\omega\mu_0 \frac{\mathrm{d}\boldsymbol{Q}}{\mathrm{d}t} : \boldsymbol{\nabla}\,\mathrm{test}(\boldsymbol{E}(\boldsymbol{R}))$, where $\boldsymbol{Q}$ is the electric quadrupole moment and $\mathrm{test}(\boldsymbol{E}(\boldsymbol{R}))$ is the test function of the electric field. As mentioned above, different orientations of the classical point sources need to be considered to calculate TPSE spectra. Fourth, the Purcell factors are determined through the integration of emitted power. For the radiative part, this integration is carried out on the inner surface of the PMLs, while for the total part (radiative plus non-radiative), it is performed on the surface of a fictional sphere with a 1.5 nm radius centered on the emitter. Fifth, an unstructured tetrahedral mesh is used, where the smallest element has a characteristic size of 0.6 nm on the structure and 0.3 nm on the sphere around the emitter. The computation of the 36 Purcell factors is performed on two workstations using an AMD Ryzen Threadripper PRO 5995WX 64-core CPU and 512GB of RAM, thus enabling their computation in parallel. For example for a triangle side length of 23 nm, the computation of one Purcell factor over 145 frequencies required 12 GB of RAM and 7.5 hours on 4 cores.

2.7 Method conclusion

We derived the interference term as a function of the dyadic Green's function in equation (9), which can be either positive or negative, resulting in an increase or a decrease of the total TPSE rate. Then, we established in equation (13) the link with the Purcell factors related to one-photon processes, enabling the classical computation of the impact of the environment via equations (14) by modeling point sources in conventional electromagnetic software packages (with e.g., finite element method [57], finite-difference time-domain method [58], etc.), as is the case for the 2ED and 2EQ transitions [42]. In other

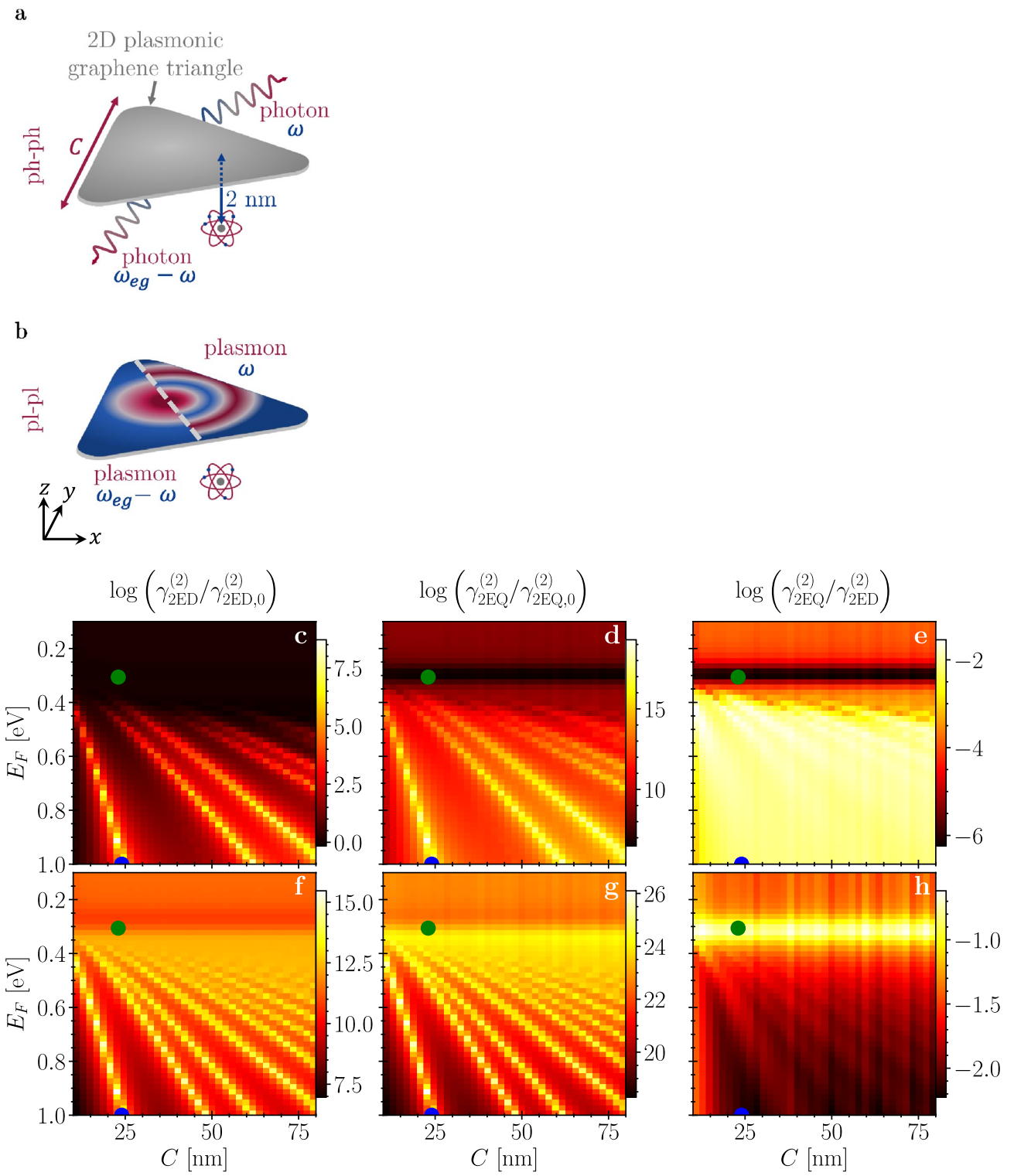

Fig. 2 **a**, **b** Sketch of the photon-photon (ph-ph, subplot **a**) and plasmon-plasmon (pl-pl, subplot **b**) emission channels of the TPSE process for a $5s \rightarrow 3s$ transition of a hydrogen-like emitter. Its transition frequency is $\hbar\omega_{eg} = 0.967$ eV (wavelength of 1.28 μm). The emitter is placed 2 nm below a 0.335 nm thickness graphene triangle of side length C. The first quantum is emitted at the frequency ω while the second one is emitted at the complementary frequency $\omega_{eg} - \omega$. **c**-**h** Ph-ph (first row) and pl-pl (second row) emission channels of the spectral TPSE rate as a function of the graphene Fermi energy E_F and of the triangle side length C at $\omega = \omega_{eg}/2$. The emitter is placed 2 nm below a corner of the structure. The green and blue dots correspond to: $E_F = 0.31$ eV, $C = 23$ nm and $E_F = 1$ eV, $C = 23.9$ nm. **c**, **f** Logarithm of the vacuum normalized spectral TPSE rate for the 2ED transition. **d**, **g** Logarithm of the vacuum normalized spectral TPSE rate for the 2EQ transition. **e**, **h** Logarithm of the ratio between the 2EQ and 2ED transition rates

words, the computation of interference between two-photon multipolar emission channels is based on the computation of interference between classical multipolar sources for both emitted quanta. Furthermore, similar equations can be derived for the interference between the other two-photon multipolar emission pathways (2MD and mixed transitions). Therefore, we have a complete framework allowing to calculate the two-photon Purcell effect of a quantum emitter in a given photonic environment up to electric quadrupolar order, with the inclusion of interference effects and valid regardless of the emitter and its environment.

In our formulas the electronic structure of the emitter (included in the second-order multipolar transition moments $\mathcal{D}^{eg}$ and $\mathcal{Q}^{eg}$) is decoupled from the influence of the photonic environment, and therefore can be calculated separately. The environment contribution involves one tensor $\mathbf{F}^{\mathrm{ED}\cap\mathrm{EQ}}$ for each emitted quantum, whose components can be either positive or negative [Eq. (13)]. Interestingly, the formulation with Purcell factors allows the separate calculation of the radiative (emission of photons to the far field) and non-radiative (absorption by the environment) emission channels to the TPSE process [26], giving access to the quantum efficiency.

3 Results and discussion

We study interference effects between two-photon multipolar emission channels during a $5s \rightarrow 3s$ transition of a hydrogen atom placed 2 nm under a two-dimensional graphene nanotriangle (see Fig. 2a, b). We have selected this structure because it is a good candidate to observe a 2EQ transition rate similar to the 2ED one [36], a necessary criterion to observe interference effects. Indeed, it was shown in Ref. [36] for one-photon spontaneous emission that the EQ transition rate can become locally 100 times larger than the dipolar one for a hydrogen-like emitter placed under the corners of a graphene nanotriangle (for specific dipole and quadrupole orientations).

Since this structure does not contribute significantly to enhancing magnetic transitions [33] and since the mixed ED–EQ and EQ–ED two-photon transitions are prohibited by selection rules between two hydrogen states that have the same azimuthal quantum number [38, 39], the total TPSE rate comprises the three contributions discussed in equation (2): 2ED, 2EQ, and their interference. Indeed, 2MD spectra have been computed (not shown) and are more than 15 orders of magnitude lower than 2EQ for all channels.

To underline the impact of interference effects on the overall TPSE rate, the following metric is used [37]:

$$R(\omega;\mathbf{R}) := \frac{\gamma^{(2)}_{\mathrm{2ED}\cap\mathrm{2EQ}}(\omega;\mathbf{R})}{\gamma^{(2)}_{\mathrm{2ED}}(\omega;\mathbf{R}) + \gamma^{(2)}_{\mathrm{2EQ}}(\omega;\mathbf{R})}. \tag{18}$$

Thus, a negative R value corresponds to destructive interference while a positive one denotes a constructive interference. Moreover, values of -1 and 1 denote fully destructive and constructive effects, respectively, while a value of 0 indicates the absence of interference. By analogy with the interference between two waves, the maximum value of R in absolute value is given by

$$R_{\mathrm{max}}(\omega;\mathbf{R}) = \frac{2\sqrt{\gamma^{(2)}_{\mathrm{2EQ}}/\gamma^{(2)}_{\mathrm{2ED}}}}{1 + \gamma^{(2)}_{\mathrm{2EQ}}/\gamma^{(2)}_{\mathrm{2ED}}}. \tag{19}$$

Thus, the closer the ratio between the 2EQ and 2ED transition rates is to 1, the greater the interference effects in the total TPSE rate can be, i.e., the larger the absolute values of R can be. For example, ratios of 10^{-1}, 10^{-2}, and 10^{-3} give $R_{\mathrm{max}} = 57.5\,\%, 19.8\,\%$, and $6.3\,\%$, respectively, while $R_{\mathrm{max}} = 10\,\%$ for a ratio equal to 2.5×10^{-3}. Thereby, a ratio of 2.5×10^{-3} between two multipolar channels indicates a possible threshold for the appearance of two-photon interference effects.

Note that in the case of 2D plasmonic infinite materials, the ratio can be written as a function of the confinement factor η: $\gamma^{(2)}_{\mathrm{2EQ}}/\gamma^{(2)}_{\mathrm{2ED}} = \eta^4\, \gamma^{(2)}_{\mathrm{2EQ},0}/\gamma^{(2)}_{\mathrm{2ED},0}$ [59], thus a threshold as a function of the confinement factor can be derived. For example, for the $2s \rightarrow 1s$ and $5s \rightarrow 3s$ transitions, the confinement factor threshold is $\eta = 215$ and 340, which are achievable values with graphene nanostructures [59, 60].

The considered system is defined by three parameters: the Fermi energy of graphene E_F, the triangle side length C, and the position of the emitter with respect to the structure. First, we show in Fig. 2c–h the 2ED and 2EQ spectral transition rates at $\omega_{eg}/2$ as a function of E_F and C in the case where the emitter is placed under a corner of the triangle. Then, these two rates and the metric R are calculated in Fig. 3 as a function of the emitter position for a specific

value of the parameters E_F and C, still at $\omega_{eg}/2$. Finally, spectra of the total TPSE rate and of R are shown in Fig. 4 and discussed for two sets of parameters, for which the surface charge density is plotted in Fig. 5.

Figure 2c–h shows the ph-ph and pl-pl emission pathways for the 2ED and 2EQ transition rates and their ratio as a function of the Fermi energy and of the structure size. For the photon-photon emission channel (first row), lines are present for the 2ED and 2EQ transitions (Fig. 2c and d) for Fermi energy roughly greater than 0.4 eV, which correspond to radiative modes excited on the structure. For the plasmon-plasmon emission channel (second row), new lines appear corresponding to non-radiative modes. Note that in this case, both dipolar and quadrupolar excitations result in the excitation of the same modes (Fig. 2f and g), but the rate enhancement is higher for the 2EQ transition (note the larger values on the scale of figures). Indeed, the maximum values for the ph-ph channel are: $\gamma^{(2)}_{2ED}/\gamma^{(2)}_{2ED,0} = 5.1 \times 10^8$, $\gamma^{(2)}_{2EQ}/\gamma^{(2)}_{2EQ,0} = 2.0 \times 10^{19}$, and $\gamma^{(2)}_{2EQ}/\gamma^{(2)}_{2ED} = 2.9 \times 10^{-2}$, while for the pl-pl channel they are: $\gamma^{(2)}_{2ED}/\gamma^{(2)}_{2ED,0} = 2.9 \times 10^{15}$, $\gamma^{(2)}_{2EQ}/\gamma^{(2)}_{2EQ,0} = 1.3 \times 10^{26}$, and $\gamma^{(2)}_{2EQ}/\gamma^{(2)}_{2ED} = 0.24$, showing a breakdown of the dipole approximation in the TPSE process since the 2EQ transition is not negligible. In contrast to the one-photon spontaneous emission process where the total EQ transition can be two orders of magnitude higher than the total ED transition for plasmon channel for transition moments parallel to the triangle [36], the TPSE process implies a summation over all possible intermediate states and therefore a summation over the emitter's orientations, including these that are less favorable to exhibit a higher ratio between the 2ED and 2EQ channels.

Furthermore, the ratio $\gamma^{(2)}_{2EQ}/\gamma^{(2)}_{2ED}$ for the pl-pl channel (Fig. 2h) is the highest in a horizontal band roughly between $E_F = 0.29$ eV and 0.36 eV, which is independent of the structure size. Indeed when the Fermi energy decreases, graphene losses increase due to interband transitions [61] (see the Figure IV.1 in the SI). Thus, the plasmons excited on the structure are rapidly absorbed, leading to a localized response independent of the structure size. Note that for Fermi energies below $E_F = 0.29$ eV, graphene assumes a dielectric behavior, rendering plasmon excitation impossible. However, we keep the notation "pl" to refer to the non-radiative channel.

The previous results were for an emitter below a triangle corner. Now we vary the emitter position, showing that interferences are indeed strongest at the corners. In Fig. 3 the ph-ph and pl-pl 2ED and 2EQ transition rates, their ratio, and the metric R are plotted for the parameters $E_F = 0.31$ eV and $C = 23$ nm, corresponding to the green dots on Fig. 2c-h (localized response, high ratio for the pl-pl channel). When two quanta of same type are emitted at the same frequency, the tensor $\mathbf{F}^{ED\cap EQ}$ appears squared in the interference term given by equation (9) and, consequently,

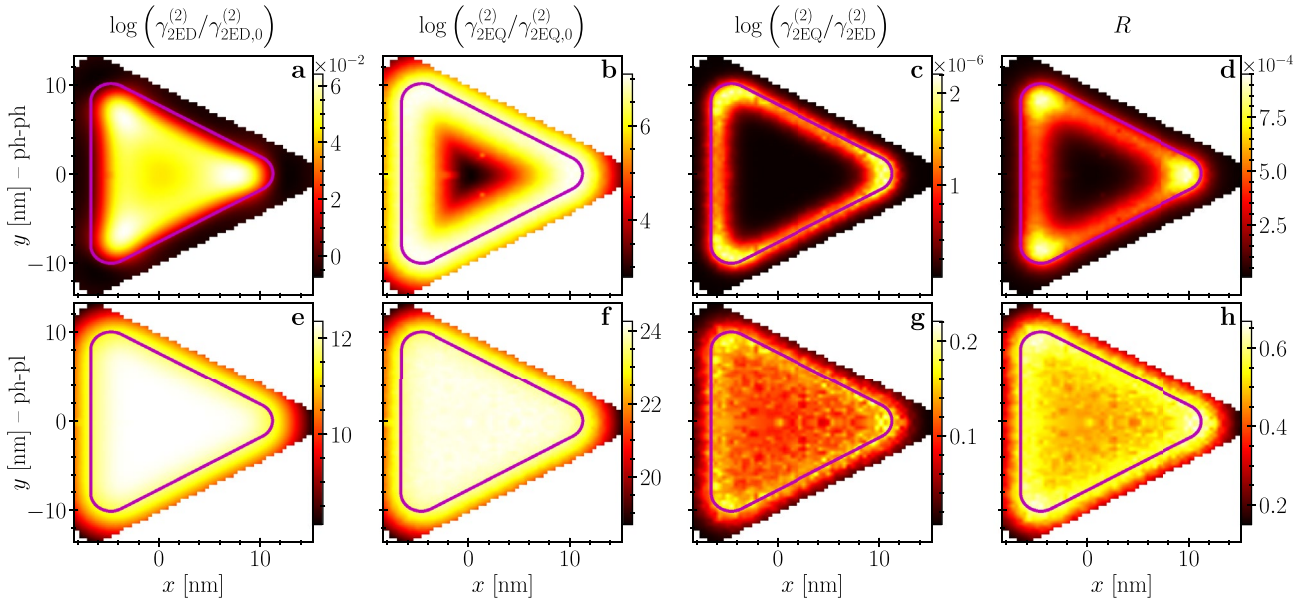

Fig. 3 Ph-ph (first row) and pl-pl (second row) emission channels of the spectral TPSE rate as a function of the emitter position at $\omega = \omega_{eg}/2$. The emitter is placed 2 nm below the structure, the graphene Fermi energy and the side length are $E_F = 0.31$ eV and $C = 23$ nm (green dots on Fig. 2c–h). A step size of 0.4 nm is used to discretize the space, leading to the computation over 435 positions on one-sixth of the triangle, since the whole figure can be retrieved using the symmetry of the structure. Note that a bilinear interpolation is used. **a**, **e** Logarithm of the vacuum normalized spectral TPSE rate for the 2ED transition. **b**, **f** Logarithm of the vacuum normalized spectral TPSE rate for the 2EQ transition. **c**, **g** Logarithm of the ratio between the 2EQ and 2ED transition rates. **d**, **h** Metric R

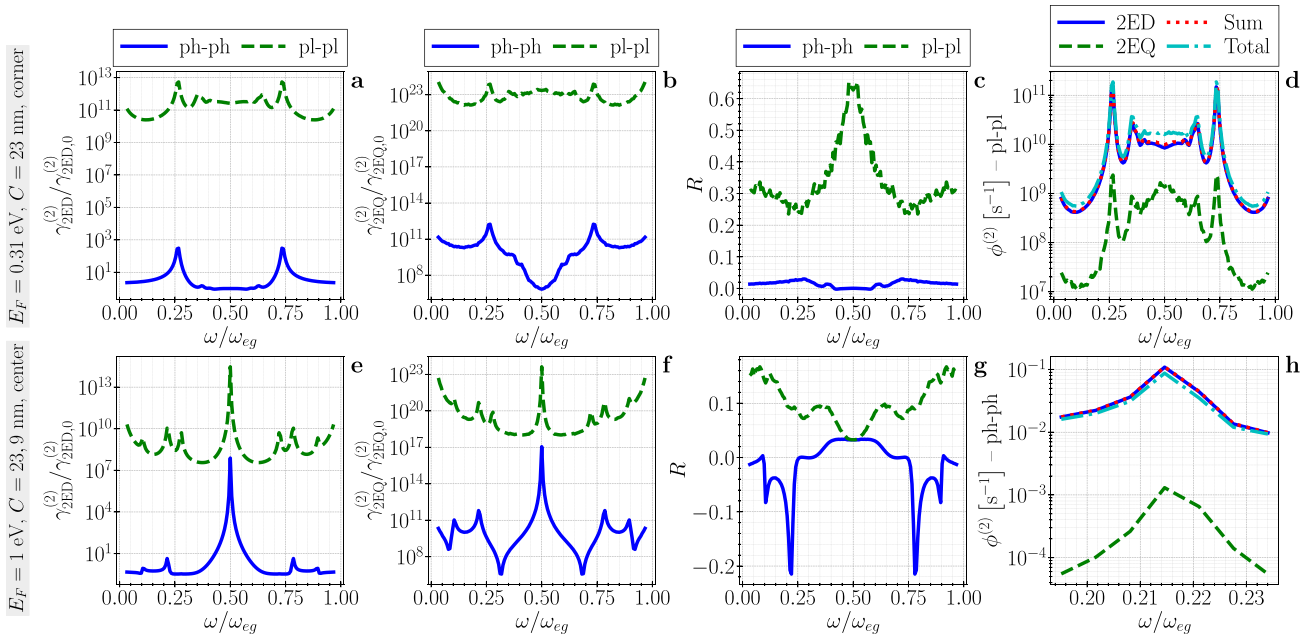

Fig. 4 Ph-ph and pl-pl emission channels of the spectral TPSE rate. For the subplots **a**-**d**, the emitter is placed 2 nm under a corner of the graphene triangle characterized by the parameters $E_F = 0.31$ eV and $C = 23$ nm (green dots on Fig. 2c–h). For the subplots **e**-**h**, the emitter is positioned 2 nm below the center of the structure that is characterized by the parameters $E_F = 1$ eV, $C = 23.9$ nm (blue dots on Fig. 2c–h). The spectra were computed over 145 frequencies. The first quantum is emitted at the frequency ω while the second one is emitted at the complementary frequency $\omega_{eg} - \omega$, leading to symmetric spectra. **a**, **e** Vacuum normalized spectral TPSE rate for the 2ED transition. **b**, **f** Vacuum normalized spectral TPSE rate for the 2EQ transition. **c**, **g** Metric R for two emission pathways. **d**, **h** Plot for the pl-pl channel (**d**) and the ph-ph channel (**h**) of the 2ED and 2EQ transition rates, the direct sum of these two, and the total transition rate, where the total one includes the interference contribution. The link between the emission profiles γ and ϕ is given by the equation (17)

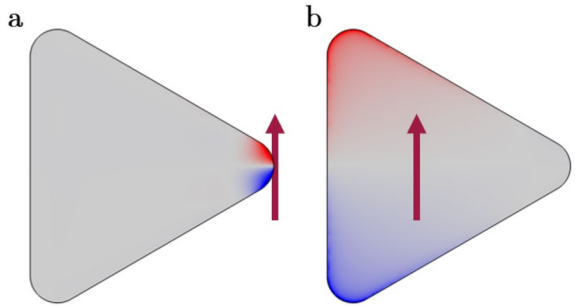

Fig. 5 Surface charge density on the graphene nanotriangle for an electric dipole oriented along the red arrow. **a** Localized response corresponding to the parameter set $E_F = 0.31$ eV and $C = 23$ nm (green dots on Fig. 2c–h), with the emitter under a corner. **b** Plasmonic mode corresponding to the parameter set $E_F = 1$ eV and $C = 23.9$ nm (blue dots on Fig. 2c–h), with the emitter under the center

the environmental contribution is always positive. Therefore, as the second-order transition moments $\mathcal{D}^{eg}$ and $\mathcal{Q}^{eg}$ involve mostly positive components [Eqs. 16], the system will always show a constructive interference.

For the photon-photon emission channel (first row), the 2ED and 2EQ transition rates present different patterns (Fig. 3a and b). For the 2ED transition, the rate is weaker than in vacuum and drops away from the structure, while for the 2EQ transition the rate is higher near the borders, especially near the corners, and decreases more slowly away from the structure to reach the vacuum value. Indeed, near the borders and particularly near the corners, there is an increased field gradient, resulting in a greater enhancement of the quadrupole interaction, resulting in a higher ratio between the 2EQ and 2ED transitions. Moreover, the metric R (Fig. 3d) is non-zero only at the borders of the structure and the highest values are at the corners. Due to the 6 orders of magnitude difference between the 2ED and 2EQ transition rates, the R values are low, with a maximum of 3×10^{-3}.

For the plasmon-plasmon emission channel (second row), the 2ED and 2EQ transition rates are fairly independent of the position below the structure (Fig. 3e and f). Moreover, R (Fig. 3h) is always non-zero under the triangle and is higher at the borders, especially near the corners. For this channel the maximum values are: $\gamma^{(2)}_{\mathrm{2EQ}}/\gamma^{(2)}_{\mathrm{2ED}} = 0.22$ and $R = 67\,\%$. Therefore, the total transition rate is 2 times higher than the 2ED transition rate, demonstrating a breakdown of the dipole approximation (the 2EQ transition is not negligible) in the TPSE process where interference effects play an important role.

The previous results showed the rate of two quanta emitted at the same frequency $\omega = \omega_{eg}/2$. Now we show TPSE spectra where constructive and destructive interferences occur. Figure 4 illustrates the spectra related to the ph-ph and pl-pl emission pathways of the 2ED and 2EQ transition rates, the metric R as well as the total TPSE rate for one channel (ph-ph or pl-pl). We employ two parameter sets: 1) $E_F = 0.31\mathrm{eV}, C = 23\,\mathrm{nm}$ (localized response illustrated in Fig. 5a, green dots on Fig. 2)c–h with the emitter under a corner; and 2) $E_F = 1\mathrm{eV}, C = 23.9\,\mathrm{nm}$ (plasmonic mode illustrated in Fig. 5b, blue dots on Fig. 2c–h) with the emitter under the center of the structure.

For the first set of parameters (first row), the interferences are always positive (Fig. 4c, $R \geq 0$), resulting in an increase in the transition rate. For the pl-pl channel (Fig. 4d) at $\omega = \omega_{eg}/2$, $\phi^{(2)}_{\mathrm{2ED}} = 8.4 \times 10^9\,\mathrm{s}^{-1}$, $\phi^{(2)}_{\mathrm{2EQ}} = 1.4 \times 10^9\,\mathrm{s}^{-1}$, $R = 63\,\%$, and $\phi^{(2)}_{\mathrm{tot}} = 1.6 \times 10^{10}\,\mathrm{s}^{-1}$. Thus, the total transition rate is 1.9 times higher than the 2ED transition rate. For the second set (second row), destructive interference occurs for the ph-ph channel (Fig. 4g, $R < 0$). For this channel (Fig. 4h) at $\omega = 0.22 \times \omega_{eg}$, $\phi^{(2)}_{\mathrm{2ED}} = 4.4 \times 10^{-2}\,\mathrm{s}^{-1}$, $\phi^{(2)}_{\mathrm{2EQ}} = 6.5 \times 10^{-4}\,\mathrm{s}^{-1}$, $R = -21\,\%$, and $\phi^{(2)}_{\mathrm{tot}} = 3.5 \times 10^{-2}\,\mathrm{s}^{-1}$. Thus, the total transition rate is 20 % lower than the 2ED transition rate, demonstrating the destructive interference.

4 Conclusion

We include interference effects between multipolar emission pathways in our framework for calculating two-photon spontaneous emission (TPSE) spectra of a quantum emitter in the vicinity of an arbitrarily shaped nanostructure. The influence of the environment is formulated in terms of Purcell factors of the one-photon spontaneous emission process, thus enabling the classical computation of the impact of the environment by modeling point sources in electromagnetic simulations. For interference terms multipolar point sources are superposed at the position of the emitter and are weighted appropriately by the multipolar vacuum TPSE rates. Therefore, the calculation of the quantum interference is carried out through the calculation of classical interference between multipolar sources. Also, when two quanta of same type are emitted at the same frequency, the system is always in a constructive interference configuration, if the second-order transition moments involve mostly positive components, as is the case for $s \rightarrow s$ transitions in hydrogen. Furthermore, interference can lead to a modification greater than 10 % of the total transition rate when the ratio between two multipolar pathways is greater than 2.5×10^{-3}, highlighting a threshold above which one needs to care about interference effects. Finally, our study focused on the interference between the two-electric dipole (2ED) and two-electric quadrupole (2EQ) transitions, but similar equations can be obtained for calculating interference between mixed and/or magnetic transitions.

Concretely, we use classical finite-element Maxwell equations' software to study TPSE for a $5s \rightarrow 3s$ transition of a hydrogen-like emitter placed 2 nm under a plasmonic graphene nanotriangle. We show a huge enhancement of the 2ED and 2EQ transitions, of 8 and 19 orders of magnitude for the emission of two photons, and of 15 and 26 orders of magnitude for the excitation of two plasmons. For the latter channel the 2EQ rate reaches 24 % of the 2ED rate, showing a breakdown of the electric dipole approximation in the TPSE process. Moreover, we find constructive and destructive interference configurations between these two pathways, with for example an increase of 67 % of the total transition rate due to the interference near the triangle corner, leading to a total transition rate being twice as large as the 2ED transition rate. Therefore, it is important to consider higher-order multipolar interactions and interference effects between multipolar two-photon transitions in systems where the field is highly confined. Experimentally, the triangular graphene nanoflakes can be synthesized [62], and the emitter-structure distance could be controlled with a transparent dielectric spacer such as NaCl [63]. The hydrogen atom is supposed here as a proof-of-concept, but more conventional emitters, such as Rydberg atoms [11] or quantum dots [41], should lead to similar conclusions.

Our framework is a complete tool to design and optimize systems for TPSE, where the exploitation of interference effects provides an additional degree of freedom. Moreover, the radiative and non-radiative channels can be calculated separately, enabling to determine the quantum efficiency. It paves the way for designing TPSE nanoantennas, just like the rich assortment that exists for single-photon emission processes [64]. For example, it can be used to design efficient entangled two-photon sources, as an alternative to the conventional parametric down-conversion sources, where the

system could emit photons of different energy in the far-field in different directions. In addition, the method can be used to study two-photon spontaneous processes for diverse and complex quantum emitters using state-of-the-art quantum mechanical methods [65] to calculate multipole moments. The emitter could be optimized to suppress the one-photon transition while increasing the two-photon one, leading to promising molecular photonic quantum technologies [66, 67].

5 Supporting information available

The Supporting Information includes the detailed derivation of the interference term betweenthe two-electric dipole and the two-electric quadrupole multipolar emission pathways as afunction of Purcell factors, a note relative to the power emitted by classical point sources,the detailed calculation of the two-electric dipole and of the two-electric quadrupole vacuumtransition rates between the 5s and 3s states of the hydrogen atom as well as the parametersof the optical response of graphene.

Author contributions All authors (S. Smeets, B. Maes, and G. Rosolen) designed the research, S. Smeets performed it, and all authors analyzed the data. The first draft of the manuscript was written by S.Smeets and all authors commented on previous versions of the manuscript. All authors read and approved the final manuscript.

Funding We acknowledge support from the FRS-FNRS (Research project T.0166.20) and from Action de Recherche Concertée (project ARC-21/25 UMONS2).

Data availibility The data that support the findings of this study are available from the corresponding author upon reasonable request.

Code availability The source code that support the findings of this study are available from the corresponding author upon reasonable request.

Declarations

Competing interests The authors declare that they have no Conflict of interest.

References

1. Hayat A, Nevet A, Ginzburg P, Orenstein M. Applications of two-photon processes in semiconductor photonic devices: invited review. Semicond Sci Technol. 2011;26: 083001.
2. Poddubny AN, Ginzburg P, Belov PA, Zayats AV, Kivshar YS. Tailoring and enhancing spontaneous two-photon emission using resonant plasmonic nanostructures. Phys Rev A. 2012;86: 033826.
3. Kwiat PG, Mattle K, Weinfurter H, Zeilinger A, Sergienko AV, Shih Y. New High-Intensity Source of Polarization-Entangled Photon Pairs. Phys Rev Lett. 1995;75:4337–41.
4. Hayat A, Ginzburg P, Orenstein M. High-rate entanglement source via two-photon emission from semiconductor quantum wells. Phys Rev B. 2007;76: 035339.
5. Hayat A, Ginzburg P, Orenstein M. Entangled Photon Spectroscopy and Communications Based on Semiconductor Two-Photon Process. International Conference on Quantum Information. Rochester, New York, 2007; p JWC63.
6. Dousse A, Suffczyński J, Beveratos A, Krebs O, Lemaître A, Sagnes I, Bloch J, Voisin P, Senellart P. Ultrabright source of entangled photon pairs. Nature. 2010;466:217–20.
7. Zhang J, Ma J, Parry M, Cai M, Camacho-Morales R, Xu L, Neshev DN, Sukhorukov AA. Spatially entangled photon pairs from lithium niobate nonlocal metasurfaces. Sci Adv. 2022;8:eabq4240.
8. Göppert-Mayer M. Über Elementarakte mit zwei Quantensprüngen. Ann Phys. 1931;401:273–94.
9. Lipeles M, Novick R, Tolk N. Direct Detection of Two-Photon Emission from the Metastable State of Singly Ionized Helium. Phys Rev Lett. 1965;15:690–3.
10. Cesar CL, Fried DG, Killian TC, Polcyn AD, Sandberg JC, Yu IA, Greytak TJ, Kleppner D, Doyle JM. Two-Photon Spectroscopy of Trapped Atomic Hydrogen. Phys Rev Lett. 1996;77:255–8.

11. Ghosh S, Rivera N, Eisenstein G, Kaminer I. Creating heralded hyper-entangled photons using Rydberg atoms. Light Sci Appl. 2021;10:100.
12. McClain, W. M. Two-photon molecular spectroscopy. Accounts of Chemical Research. 7, 129–135. Publisher: American Chemical Society; 1974.
13. Ota Y, Iwamoto S, Kumagai N, Arakawa Y. Spontaneous Two-Photon Emission from a Single Quantum Dot. Phys Rev Lett. 2011;107: 233602.
14. Dovzhenko D, Krivenkov V, Kriukova I, Samokhvalov P, Karaulov A, Nabiev I. Enhanced spontaneous emission from two-photon-pumped quantum dots in a porous silicon microcavity. Opt Lett. 2020;45:5364.
15. Wang C-F, Mantilla ABC, Gu Y, El-Khoury PZ. Ambient Tip-Enhanced Two Photon Photoluminescence from CdSe/ZnS Quantum Dots. J Phys Chem A. 2023;127:1081–4.
16. Hayat A, Ginzburg P, Orenstein M. Observation of two-photon emission from semiconductors. Nat Photonics. 2008;2:238–41.
17. van Driel HM. On the path to entanglement. Nat Photonics. 2008;2:212–3.
18. Nevet A, Berkovitch N, Hayat A, Ginzburg P, Ginzach S, Sorias O, Orenstein M. Plasmonic Nanoantennas for Broad-Band Enhancement of Two-Photon Emission from Semiconductors. Nano Lett. 2010;10:1848–52.
19. Hu F, Li L, Liu Y, Meng Y, Gong M, Yang Y. Two-plasmon spontaneous emission from a nonlocal epsilon-near-zero material. Commun Phys. 2021;4:84.
20. Muniz Y, Manjavacas A, Farina C, Dalvit DAR, Kort-Kamp WJM. Two-Photon Spontaneous Emission in Atomically Thin Plasmonic Nanostructures. Phys Rev Lett. 2020;125: 033601.
21. Whisler C, Holdman G, Yavuz DD, Brar VW. Enhancing two-photon spontaneous emission in rare earths using graphene and graphene nanoribbons. Phys Rev B. 2023;107: 195420.
22. Weitzel L, Muniz Y, Farina C, Zarro CA. Two-photon spontaneous emission of an atom in a cosmic string background. Phys Rev D. 2022;106: 045020.
23. Klimov VV. Control of the emission of elementary quantum systems using metamaterials and nanometaparticles. Phys Usp. 2021;64:990–1020.
24. Rivera N, Kaminer I, Zhen B, Joannopoulos JD, Soljačić M. Shrinking light to allow forbidden transitions on the atomic scale. Science. 2016;353:263–9.
25. Purcell EM, Torrey HC, Pound RV. Resonance Absorption by Nuclear Magnetic Moments in a Solid. Phys Rev. 1946;69:37–8.
26. Novotny L, Hecht B. Principles Nano-Opt. 2nd ed. Cambridge: Cambridge University Press; 2012.
27. Rivera N, Kaminer I. Light-matter interactions with photonic quasiparticles. Nat Rev Phys. 2020;2:538–61.
28. Andersen ML, Stobbe S, Sørensen AS, Lodahl P. Strongly modified plasmon-matter interaction with mesoscopic quantum emitters. Nat Phys. 2011;7:215–8.
29. Jain PK, Ghosh D, Baer R, Rabani E, Alivisatos AP. Near-field manipulation of spectroscopic selection rules on the nanoscale. Proc Natl Acad Sci. 2012;109:8016–9.
30. Kern AM, Martin OJF. Strong enhancement of forbidden atomic transitions using plasmonic nanostructures. Phys Rev A. 2012;85: 022501.
31. Yannopapas V, Paspalakis E. Giant enhancement of dipole-forbidden transitions via lattices of plasmonic nanoparticles. J Mod Opt. 2015;62:1435–41.
32. Marquier F, Sauvan C, Greffet J-J. Revisiting Quantum Optics with Surface Plasmons and Plasmonic Resonators. ACS Photonics. 2017;4:2091–101.
33. Sanders S, May A, Alabastri A, Manjavacas A. Extraordinary Enhancement of Quadrupolar Transitions Using Nanostructured Graphene. ACS Photonics. 2018;5:3282–90.
34. Neuman T, Esteban R, Casanova D, García-Vidal FJ, Aizpurua J. Coupling of Molecular Emitters and Plasmonic Cavities beyond the Point-Dipole Approximation. Nano Lett. 2018;18:2358–64.
35. Kosik M, Burlayenko O, Rockstuhl C, Fernandez-Corbaton I, Słowik K. Interaction of atomic systems with quantum vacuum beyond electric dipole approximation. Sci Rep. 2020;10:5879.
36. Rosolen G, Maes B. Strong multipolar transition enhancement with graphene nanoislands. APL Photonics. 2021;6: 086103.
37. Rusak E, Straubel J, Gładysz P, Göddel M, Kędziorski A, Kühn M, Weigend F, Rockstuhl C, Słowik K. Enhancement of and interference among higher order multipole transitions in molecules near a plasmonic nanoantenna. Nat Commun. 2019;10:5775.
38. Cowan RD. The theory of atomic structure and spectra; Los Alamos series in basic and applied sciences 3. Berkeley: University of California Press; 1981.
39. Goldman SP, Drake GWF. Relativistic two-photon decay rates of $2s_{1/2}$ hydrogenic ions. Phys Rev A. 1981;24:183–91.
40. Craig DP, Thirunamachandran T. Molecular quantum electrodynamics: an introduction to radiation-molecule interactions; Academic Press: London ; Orlando, 1984
41. Tighineanu P, Andersen ML, Sørensen AS, Stobbe S, Lodahl P. Probing Electric and Magnetic Vacuum Fluctuations with Quantum Dots. Phys Rev Lett. 2014;113: 043601.
42. Smeets S, Maes B, Rosolen G. General framework for two-photon spontaneous emission near plasmonic nanostructures. Phys Rev A. 2023;107: 063516.
43. Muniz Y, da Rosa FSS, Farina C, Szilard D, Kort-Kamp WJM. Quantum two-photon emission in a photonic cavity. Phys Rev A. 2019;100: 023818.
44. Zhang Y, Dong Z-C, Aizpurua J. Influence of the Chemical Structure on Molecular Light Emission in Strongly Localized Plasmonic Fields. J Phys Chem C. 2020;124:4674–83.
45. Barron LD, Gray CG. The multipole interaction Hamiltonian for time dependent fields. J Phys A: Math Nucl Gen. 1973;6:59–61.
46. Grosjean T, Mivelle M, Baida FI, Burr GW, Fischer UC. Diabolo Nanoantenna for Enhancing and Confining the Magnetic Optical Field. Nano Lett. 2011;11:1009–13.
47. Milonni PW. The quantum vacuum: an introduction to quantum electrodynamics. Boston: Academic Press; 1994.
48. Cohen-Tannoudji C, Diu B, Laloë F. Quantum mechanics. Volume 3: Fermions, bosons, photons, correlations and entanglement, first edition ed.; Wiley-VCH GmbH & Co. KGaA: Weinheim, 2020.
49. Chluba J, Sunyaev RA. Two-photon transitions in hydrogen and cosmological recombination. Astronomy Astrophys. 2008;480:629–45.
50. Bethe HA, Salpeter EE. Quantum Mechanics of One- and Two-Electron Atoms; Springer. Berlin Heidelberg: Berlin, Heidelberg; 1957.

51. Matsumoto A. Multipole matrix elements for hydrogen atom. Phys Scr. 1991;44:154–7.
52. Jackson JD. Classical electrodynamics. 3rd ed. New York: Wiley; 1999.
53. Xinzhong TC. Modeling Graphene in High-Frequency Electromagnetics. 2022; https://www.comsol.com/blogs/modeling-graphene-in-high-frequency-electromagnetics/
54. Yang G, Li L, Lee WB, Ng MC. Structure of graphene and its disorders: a review. Sci Technol Adv Mater. 2018;19:613–48.
55. Falkovsky LA, Varlamov AA. Space-time dispersion of graphene conductivity. Eur Phys J B. 2007;56:281–4.
56. Falkovsky LA. Optical properties of graphene. J Phys: Conf Ser. 2008;129: 012004.
57. Jin J-M. The finite element method in electromagnetics, third edition ed.; John Wiley & Sons Inc: Hoboken. New Jersey, 2014.
58. Taflove A, Hagness SC. Computational electrodynamics: the finite-difference time-domain method. 3rd ed. Boston: Artech House antennas and propagation library; Artech House; 2005.
59. Rivera N, Rosolen G, Joannopoulos JD, Kaminer I, Soljačić M. Making two-photon processes dominate one-photon processes using mid-IR phonon polaritons. Proc Natl Acad Sci. 2017;114:13607–12.
60. Diaconescu B, Pohl K, Vattuone L, Savio L, Hofmann P, Silkin VM, Pitarke JM, Chulkov EV, Echenique PM, Farias D, Rocca M. Low-energy acoustic plasmons at metal surfaces. Nature. 2007;448:57–9.
61. Koppens FH, Chang DE, García Abajo FJ. Graphene plasmonics: a platform for strong light–matter interactions. Nano Lett. 2011;11(8):3370–7.
62. Mishra S, Beyer D, Eimre K, Liu J, Berger R, Gröning O, Pignedoli CA, Müllen K, Fasel R, Feng X, Ruffieux P. Synthesis and Characterization of π-Extended Triangulene. J Am Chem Soc. 2019;141:10621–5.
63. Rosławska A, Neuman T, Doppagne B, Borisov AG, Romeo M, Scheurer F, Aizpurua J, Schull G. Mapping Lamb, Stark, and Purcell Effects at a Chromophore-Picocavity Junction with Hyper-Resolved Fluorescence Microscopy. Phys Rev X. 2022;12: 011012.
64. Koenderink AF. Single-Photon Nanoantennas. ACS Photonics. 2017;4:710–22.
65. Parr RG, Weitao Y. Density-Functional Theory of Atoms and Molecules; Oxford University Press, 1995.
66. Murtaza G, Colautti M, Hilke M, Lombardi P, Cataliotti FS, Zavatta A, Bacco D, Toninelli C. Efficient room-temperature molecular single-photon sources for quantum key distribution. Opt Express. 2023;31:9437.
67. Duquennoy R, Colautti M, Emadi R, Majumder P, Lombardi P, Toninelli C. Real-time two-photon interference from distinct molecules on the same chip. Optica. 2022;9:731.